



# Non-uniform muscle fat replacement along the proximodistal axis in Duchenne muscular dystrophy

M.T. Hooijmans<sup>a,\*</sup>, E.H. Niks<sup>b</sup>, J. Burakiewicz<sup>a</sup>, C. Anastasopoulos<sup>a,c</sup>, S.I. van den Berg<sup>b</sup>,  
E. van Zwet<sup>d</sup>, A.G. Webb<sup>a</sup>, J.J.G.M. Verschuuren<sup>b</sup>, H.E. Kan<sup>a</sup>

<sup>a</sup> C.J. Gorter Center for High Field MRI, Dept. of Radiology, Leiden University Medical Center, Zuid-Holland, Netherlands

<sup>b</sup> Dept. of Neurology, Leiden University Medical Center, Leiden, Zuid-Holland, Netherlands

<sup>c</sup> Dept. of Neuropediatrics and Muscle Disorders, University of Freiburg, Freiburg, Germany

<sup>d</sup> Dept. of Biostatistics, Leiden University Medical Center, Leiden, Zuid-Holland, Netherlands

Received 31 August 2016; received in revised form 14 February 2017; accepted 15 February 2017

## Abstract

The progressive replacement of muscle tissue by fat in Duchenne muscular dystrophy (DMD) has been studied using quantitative MRI between, but not within, individual muscles. We studied fat replacement along the proximodistal muscle axis using the Dixon technique on a 3T MR scanner in 22 DMD patients and 12 healthy controls. Mean fat fractions per muscle per slice for seven lower and upper leg muscles were compared between and within groups assuming a parabolic distribution. Average fat fraction for a small central slice stack and a large coverage slice stack were compared to the value when the stack was shifted one slice (15 mm) up or down. Higher fat fractions were observed in distal and proximal muscle segments compared to the muscle belly in all muscles of the DMD subjects ( $p < 0.001$ ). A shift of 15 mm resulted in a difference in mean fat fraction which was on average 1–2% ranging up to 12% ( $p < 0.01$ ). The muscle end regions are exposed to higher mechanical strain, which points towards mechanical disruption of the sarcolemma as one of the key factors in the pathophysiology. Overall, this non-uniformity in fat replacement needs to be taken into account to prevent sample bias when applying quantitative MRI as biomarker in clinical trials for DMD.

© 2017 Elsevier B.V. All rights reserved.

**Keywords:** MRI; Muscle; Fat replacement; DMD

## 1. Introduction

Duchenne muscular dystrophy (DMD) is caused by a mutation in the *DMD* gene and is characterized by progressive muscle weakness [1]. Quantitative MRI is becoming increasingly important as a non-invasive method to follow disease progression, and is considered a promising surrogate outcome measure for clinical trials [2]. Assessment of fat replacement in individual muscles and in relation to clinical outcomes has been studied extensively by MRI [3–17].

The fat fraction of a muscle is normally calculated from the average of several central slices in a muscle [7,8,11], or of a specific region of interest [17,18]. However, it is unknown if fat is distributed uniformly over the muscle, and thus how robust

this type of measurement is with respect to the exact location over which the images are quantified. For example, in Charcot–Marie–Tooth disease and facio-scapulo-humeral muscular dystrophy, it is known that fat replacement varies along the proximodistal axis [19,20]. In DMD it is plausible that fat distribution is non-uniform, as dystrophin is non-uniformly distributed [21], and mechanical strain is highest in the muscle end regions [22–24]. This non-uniformity potentially has a major effect on the calculated fat fraction, particularly since in longitudinal studies DMD boys inevitably grow in-between examinations and accurate repositioning is very challenging. In this study, therefore, we 1) assessed the distribution of fat replacement along the proximodistal muscle axis, and 2) determined the effect of a slight shift in spatial localization along the proximodistal muscle axis on the measured mean fat fraction in DMD boys using two commonly used approaches: analysis of a small central slice stack or volume [3,4,6,10,17] and analysis of a non-contiguous slice stack with a large coverage in feet head direction [7,11,12,15].

\* Corresponding author. Department of Radiology, C-03-Q, LUMC, Albinusdreef 2, 2333 ZA Leiden, Netherlands. Fax: +31 72 5268256.

E-mail address: [m.t.hooijmans@lumc.nl](mailto:m.t.hooijmans@lumc.nl) (M.T. Hooijmans).

## 2. Methods

### 2.1. Participants

Twenty-two DMD patients (mean age  $9.3 \pm 3.1$  years, range 5–16 years) and twelve healthy control subjects ( $9.7 \pm 2.9$  years, range: 5–14 years) participated in this study. Patients were recruited from the Dutch Dystrophinopathy database [25]. Exclusion criteria were MRI contraindications and the inability to lie supine for at least 30 minutes. Diagnosis was confirmed by molecular genetic testing. Among the DMD patients, 16 were fully ambulant, 6 patients were wheelchair bound and all patients used corticosteroids with intermittent dosing regimens (varying between 8 and 10 days on/off). Healthy controls were recruited from local schools and sport clubs. The study was approved by the local medical ethics committee, and written informed consent was obtained from all subjects and their parents.

### 2.2. MR methods

MR images were acquired in the right lower and upper leg on a 3T MR system (Ingenia, Philips Healthcare, Best, The Netherlands), using a 16-channel body receive coil array placed on top of the legs in combination with the 12-channel receive coil array located within the patient table. Patients were positioned in a feet first, supine position. The coil was placed on top of the leg in order to cover the full length of the upper and lower leg. In the taller boys, the coil had to be repositioned during scanning to ensure full coverage of the upper leg. The imaging protocol contained a 3D survey scan for localization, transmit field ( $B_1^+$ ) calibration and 3-Point Gradient Echo Dixon to determine fat replacement (23 slices; voxel size  $1 \times 1 \times 10$  mm; interslice gap 5 mm; repetition time (TR)/echo time (TE)/echo time shift ( $\Delta TE$ ) 210/4.41/0.76 ms; 2 signal averages and a flip angle of  $8^\circ$ ). All scans were aligned to the tibia and femur bone, and positioned in such a way as to provide maximal coverage of the muscles in the lower and upper leg.

### 2.3. Data-analysis

Fat and water images were generated using a multi-peak model based on a six fat peak spectrum coded in Matlab (Mathworks, Natick, MA, USA). Values were not corrected for  $T_2^*$  relaxation effects [26,27]. The sequence was optimized with respect to TR and flip angle to avoid  $T_1$  relaxation effects. After reconstruction, visual inspection was used to assess image quality to detect reconstruction failure, B0 artefacts and movement artefacts. Images with clear artefacts were removed from further analysis.

Regions of interest (ROIs) were drawn manually using Medical Image Processing, Analysis and Visualization (MIPAV) software (<http://mipav.cit.nih.gov>) for seven individual lower and upper leg muscles for which full coverage of the muscle was achieved within the field-of-view of the Dixon scan, namely the soleus (SOL), the tibialis anterior (TA), the peronei (PER), the tibialis posterior (TP), the extensor digitorum longus (EDL), the vastus lateralis (VL) and the biceps femoris long head (BFL) muscle. ROIs were drawn on the reconstructed water images. The boundaries of the ROIs

were chosen to always fall within a muscle in order to avoid contamination of subcutaneous fat and fatty intermuscular septa. In the more severely affected patients, both the reconstructed fat and water images were used to ensure that the boundaries of the ROI fell within the muscle. ROIs were only drawn on slices in which the muscle was visible. Quantitative fat fractions were calculated as signal intensity (SI) fat/(SI fat + SI water)\*100 from the reconstructed fat and water images and reported as a mean value of all pixels within a ROI. Fat fraction (%) was calculated per ROI and per slice. For visual comparison of fat distribution along the proximodistal muscle axis between subjects of different ages, all datasets were aligned according to their maximal cross-sectional area of the muscle (maxCSA).

### 2.4. Statistical analysis

Generalized Estimating Equations (GEE) were used to assess the fat distribution pattern in both groups separately, assuming a parabolic curvature ( $ax^2 + bx + c$ ). GEE was also used to assess differences in fat distribution pattern along the proximodistal muscle axis between DMD patients and healthy controls. GEE takes into account the repeated measurements within the same muscle (individual slices).

Differences in mean fat fraction between measurement locations within an individual muscle were assessed using a paired t-test for Small Coverage (SC) and Large Coverage (LC) analyses. For the SC analysis, the mean fat fraction was averaged over four central slices. The first location was at the thickest part of the calf or at mid-thigh level. For the second and third locations, the selection of slices was shifted one slice in the distal direction or one slice in the proximal direction in relation to the first location. All three locations along the proximodistal muscle axis covered the same distance (5.5 cm) of the calf. For the LC analysis, the mean fat fraction was averaged over 5 non-consecutive slices. The middle slice of the stack was positioned at the thickest part of the leg or at mid-thigh level for the first location. For the second and third locations, the selection of slices was shifted one slice proximal and one slice distal in relation to the first location. All three locations along the proximodistal muscle axis covered the same distance (13 cm) of the calf.

Finally, a Bland–Altman plot was used to assess the difference between the fat fraction calculated at the central slices and fat fraction calculated over the whole muscle. A Bonferroni correction was applied to correct for multiple comparisons resulting in a significance level set of  $p < 0.01$  in the paired analysis and a significance level set of  $p < 0.002$  in the GEE analysis. Statistical analyses were performed using SPSS version 20 for Windows (SPSS Inc., Chicago).

## 3. Results

Full lower leg datasets were obtained in all DMD patients and healthy controls. Upper leg datasets were acquired in all healthy controls and in 16 DMD patients. In six DMD patients, the protocol could not be completed due to fatigue, patient discomfort in the supine lying position, or anxiety upon

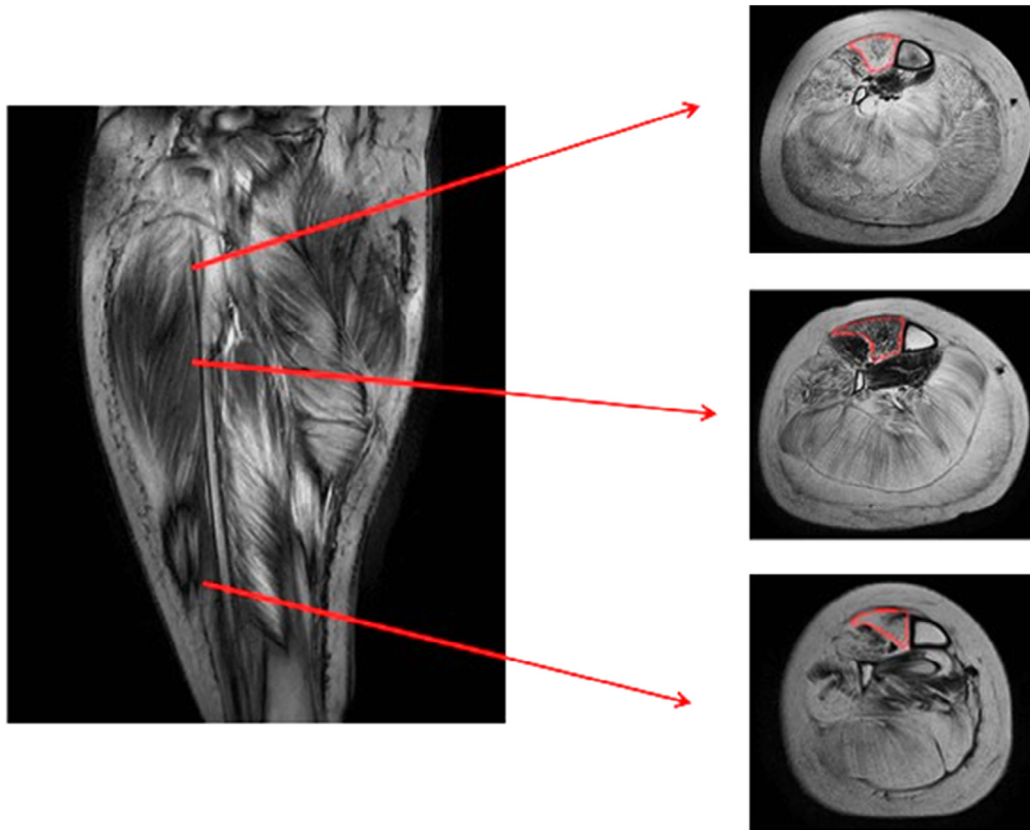


Fig. 1. Fat reconstruction of the right lower leg of a DMD patient in the coronal and axial plane. Note the distribution of fat along the proximodistal muscle axis of the TA muscle (red arrows). Together with three axial fat-only images showing a distal, middle and proximal muscle section of the TA muscle visualized with a manually drawn ROI (red). The middle slice has, already visually, less fat replacement compared to the proximal and distal slice.

entrance into the scanner bore. Five upper leg datasets (two DMD patients and three healthy control subjects) and one lower leg dataset (HC subject) had to be excluded due to movement artefacts. In all cases, the two outer slices on both sides were excluded from the analysis due to reconstruction failure caused by  $B_0$  inhomogeneities.

### 3.1. Fat distribution over the entire length of the muscle

Within-group analysis showed that the fat distribution pattern along the proximodistal muscle axis was non-uniform in patients and controls. Higher fat fractions were observed in the

more proximal and distal muscle parts compared to the maxCSA (Figs. 1 and 2a,b). The fat distribution pattern could be well described by a parabolic curvature for all the analysed muscles of the DMD patients (range in  $a$ : 0.133–0.390;  $p < 0.001$ ) and healthy controls (range in  $a$ : 0.003–0.084;  $p < 0.001$ ), with the exception of the PER muscle ( $a = 0.003$ ;  $p = 0.858$ ). Between-group analysis showed a significantly more pronounced parabolic fat distribution pattern in DMD patients compared to healthy controls for all muscles analysed ( $p < 0.001$ ), with the exception of the BFL muscle (DMD  $a = 0.133$ ; HC  $a = 0.084$ ;  $p = 0.176$ ).

Table 1

The mean, standard deviation and the absolute range of the difference in %fat for a slight shift in location along the axis in the DMD patients for the large coverage (LC) and the small coverage (SC) analyses. SC/LC – Distal: the difference between mean fat fraction obtained at the thickest part of the calf or at mid-thigh level and that obtained when shifted one slice in the distal direction. SC/LC – Proximal: the difference between mean fat fraction obtained at the thickest part of the calf or at mid-thigh level and that obtained when shifted one slice in the proximal direction. Significant differences are indicated with \*.

Muscle	LC – Distal	LC – Proximal	SC – Distal	SC – Proximal
EDL	1.4 ± 2.3 (0.04–6.9%)*	2.9 ± 3 (0.03–10.7%)	−1.5 ± 2.8 (0.06–12%)*	0.4 ± 3.1 (0.01–10.7%)
PER	−0.2 ± 2.9 (0.17–4.1%)*	2.1 ± 1.9 (0.7–7.8%)*	−2.5 ± 1.9 (0.12–5.2%)*	1.4 ± 3.6 (0.67–11.3%)*
SOL	−1.0 ± 2 (0.03–3.7%)*	3.1 ± 2.6 (0.01–3.26%)*	−1 ± 1.8 (0.03–6.1%)*	−0.06 ± 1.6 (0.01–3.26%)
TA	0.2 ± 2.6 (0.16–9.3%)*	2.3 ± 2.8 (0.4–8.4%)*	−1.3 ± 2.2 (0.16–9.1%)*	−0.02 ± 2.2 (0.02–5.3%)
TP	0.5 ± 0.6 (0.04–2.1%)*	0.9 ± 0.8 (0.07–3.37%)*	−0.21 ± 0.7 (0.04–2.1%)	−0.2 ± 1.1 (0.07–3.37%)
BFL	0.9 ± 1.4 (0.03–4.4%)*	0.4 ± 1.2 (0.15–3%)	0.7 ± 1.7 (0.21–4.2%)*	−1.6 ± 2.2 (0.32–7%)*
VL	1.7 ± 1.9 (0.25–6.2%)*	0.4 ± 1.1 (0.02–1.7%)	1.0 ± 1.5 (0.04–3.96%)	−1.6 ± 1.6 (0.3–5%)*

Abbreviations: TA, tibialis anterior; TP, tibialis posterior; EDL, extensor digitorum longus; PER, peroneal muscles; SOL, soleus; VL, vastus lateralis; BFL, biceps femoris long head.

### 3.2. Differences in fat fraction with a slight shift in positioning

Shifting the slices which were analysed by one slice either in the proximal or distal direction resulted in a significant

difference in fat fraction for the majority of the muscles for both the SC and LC analyses (Table 1). The difference was on average 1.7% and up to 12% for the SC analysis (Fig. 2c,d) and 1.7% ranging up to 10.7% for the LC analysis (Fig. 2e,f). The Bland–Altman plot of the central slice fat fraction versus whole

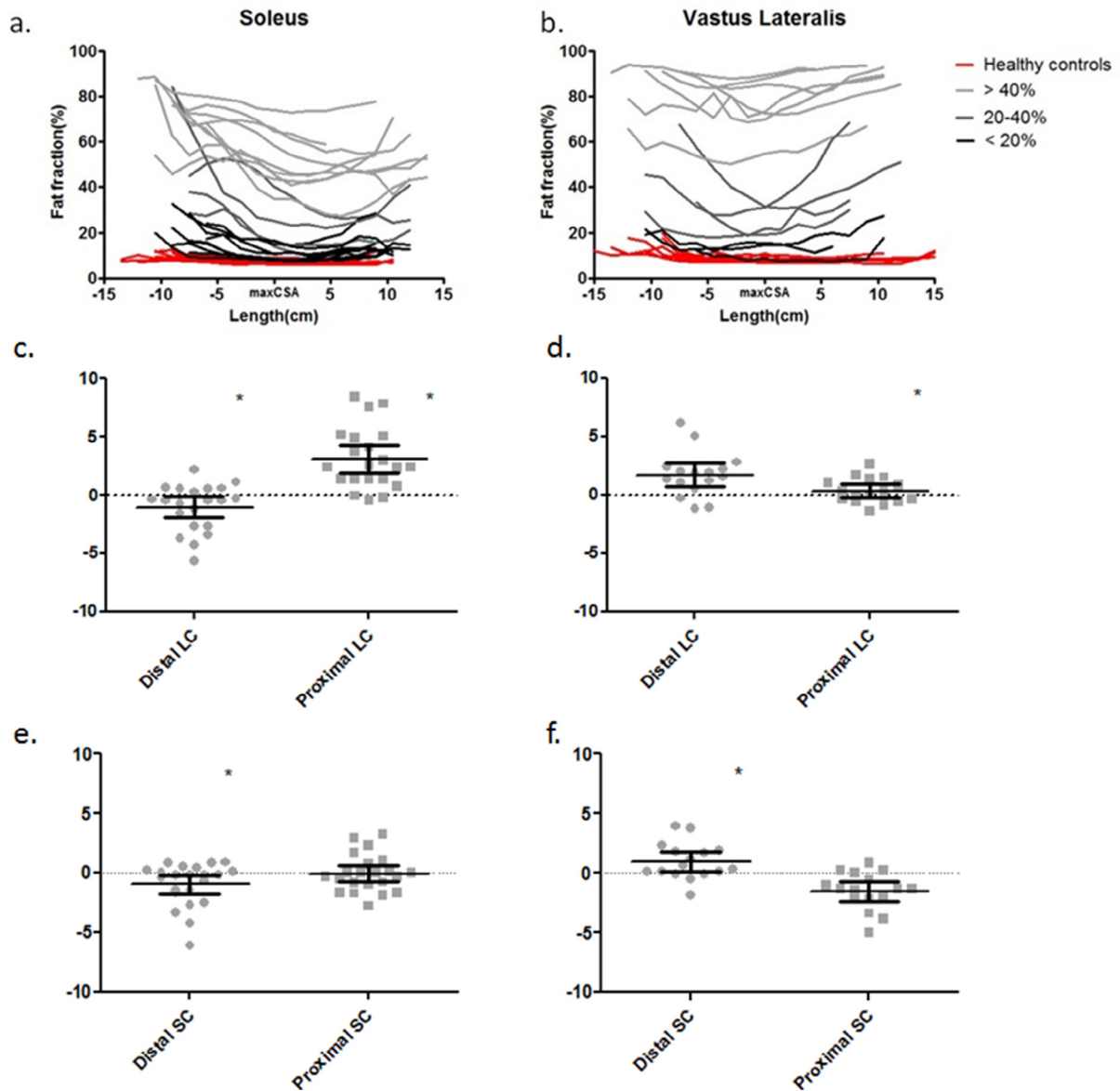


Fig. 2. Fat distribution over the entire length of the muscle and the difference in fat fraction due to a slight shift in positioning. Fat fraction (% fat) as a function of location (cm) along the proximodistal muscle axis (a) for the SOL muscle (b) and the VL muscle. The middle point of the graph is aligned with the maximal Cross Sectional Area (maxCSA) of the muscle in order to facilitate visual comparisons between subjects. The left direction shows the more distal muscle part while the right direction showed the proximal muscle part. Due to natural variation in length, as well as leg and muscle size, the amount of data points plotted on both sides of the maxCSA varied per subject and per muscle. Each line represents one individual subject. To increase the readability of the graphs DMD patients are grouped and coloured according to their mean fat fraction (red = HC subjects, black = %fat < 20, dark grey = 20 < %fat < 40, light grey = %fat > 40%). This grouping according to mean fat fraction is only for visual support and not part of the statistical analysis. Differences in mean fat fraction (c–e) for the SOL muscle (d–f) and the VL muscle for the small coverage (SC) and large coverage (LC) analyses. SC/LC – Distal: the difference between mean fat fraction obtained at the thickest part of the calf or at mid-thigh level and that obtained when shifted one slice in the distal direction. SC/LC – Proximal: the difference between mean fat fraction obtained at the thickest part of the calf or at mid-thigh level and that obtained when shifted one slice in the proximal direction. Each grey square/dot represents one individual DMD subject. The black bars represent the mean and 95% CI. Significant differences are indicated with \*. Note the more homogeneous fat distribution along the proximodistal muscle axis in the higher affected DMD patients in the VL muscle together with the high variation when the analysis window was shifted one slice proximal or distal.

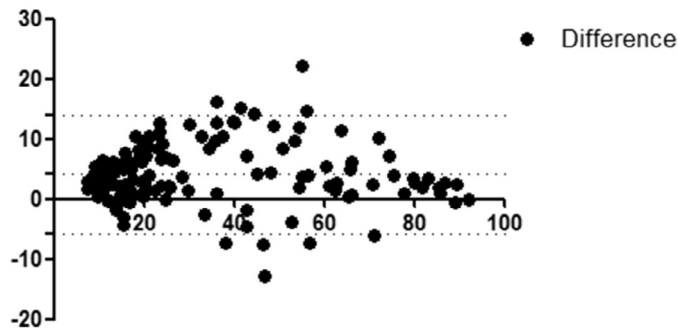


Fig. 3. Difference between whole muscle fat fraction and the averaged fat fraction. Bland–Altman plot of the difference in fat fraction between whole muscle measurement and the averaged fat fraction over the four middle slices. Each square represents one individual muscle of an individual subject. Note the increase in the difference between the two methods in the intermediate fat fractions.

muscle fat fraction showed that the largest differences in mean fat fraction (i.e. between 0.13% and 22.24%) occurred in muscles with intermediate fat fractions (Figs. 2a,b and 3).

#### 4. Discussion

Our results show that in DMD patients all analysed leg muscles have a non-uniform fat distribution pattern along the proximodistal muscle axis, showing higher fat replacement near the origin and insertion of the muscle compared to the muscle belly. This specific pattern is also found in the muscles of the healthy control subjects, although significantly less prominent.

The non-uniform fat fraction has important implications for the use of quantitative MRI or MR spectroscopy of fat replacement or muscle biopsies as biomarkers in clinical trials [2]. Our study has shown that a slight shift of 1.5 cm along the proximodistal muscle axis results in significant differences in estimated mean fat fraction. Importantly, these differences are in the same range (SC analysis average: 1.7% up to 12%; LC analysis average: 1.2% up to 11%) as changes found in fat fraction in longitudinal studies over a 12 or 18 month time period [8,11,13–15,17]. Due to the parabolic shape of the fat distribution along the proximodistal muscle axis, a shift in slice spacing to either the proximal or the distal side of the muscle will result in an artificial increase of the measured fat fraction when the slice stack is positioned at the lowest point of the parabola. As a result, this sample bias is independent of the shift direction and cannot be averaged out. However, this is not always the case since usually slice stacks are positioned at a specific distance from a bony landmark. As this will not directly match to the lowest point of the parabola for each muscle, it is possible that the difference will be averaged out on a group level. Overall, this greatly diminishes the discriminant power of the technique and stresses the need for extreme accurate and reproducible spatial localization over time.

Fat replacement is commonly assessed using MR by 2D or 3D imaging or MR spectroscopy [7,8,11,18]. The intrinsic parameters involved in this methodology, i.e. slice gaps, slice thickness, field-of-view and restricted voxel size, could result in

limited and location-specific information on the fat fraction. In addition, due to the age of DMD boys in current clinical trials, boys will inevitably grow during the trial. Both aspects complicate spatial localization in a longitudinal study setup. Using a combination of bony landmarks, internal muscle references, and external references such as fish oil capsules placed on the skin is recommended to increase accuracy [28,29]. Ultimately, a 3D acquisition that covers the whole limb will be the most robust method to acquire data in a longitudinal follow-up. The full coverage allows accurate offline matching of datasets.

Another implication of the non-uniform distribution of fat with respect to the use of MRI in clinical trials is the less prominent parabolic curvature in muscles with either high or low fat fractions compared to intermediately affected muscles. These differences in parabolic curvature are most likely caused by evolution of the fat distribution pattern over time from a homogeneous initial phase (unaffected muscle) through a heterogeneous middle state (intermediate affected muscle) to a homogeneous end stage (highly affected muscle). This effect can also be visualized in the Bland–Altman plot, where more prominent differences in mean fat fraction between the central four slices and the whole muscle fat fraction were observed in the intermediate affected muscles compared to the un-affected and highly affected muscles. Therefore, the highest bias due to sampling errors occurs in these intermediate affected muscles. However, these muscles in particular are the ones which are most likely to be useful as a surrogate endpoint in clinical trials, as they have the highest potential of showing a response to treatment via a decrease in the rate of progression of fat replacement.

In addition to the clinical implications of measuring the non-uniform nature of the fat distribution, this type of measurement could help in the understanding of the underlying pathophysiology in DMD. In healthy skeletal muscle, mechanical strain is non-uniformly distributed along the proximodistal muscle axis, where higher strain is observed in the muscle end regions compared to the muscle belly [23,24,30]. In healthy mice, dystrophin has been shown to be particularly concentrated near these end regions [31] in contrast to other proteins associated with mechanical stability such as connectin and nebulin [32]. In addition, dystrophin-deficient muscles are especially susceptible to stretch-induced muscle injury [33,34]. It therefore seems logical that mechanical disruption of the membrane might be one of the key causative factors for muscle degeneration and for fat replacement in DMD to evolve more prominently in the end regions compared to the muscle belly.

Our study had some limitations. In the reconstruction of the three-point Dixon images, no T2\* correction was applied which could result in an overestimation of the fat fractions in the low fat ranges [27]. However, as this will result in artificially high fat fractions in the low fat range, correcting for T2\* would only result in an even more pronounced parabolic curvature. Secondly, in this work only the seven lower and upper leg muscles of which full coverage could be ensured have been analysed. In the upper leg in particular the field-of-view was not

large enough to cover entire muscles and the B0 artefacts near the joints prevented analysis of bi-articular muscles. This could have resulted in a selection bias towards shorter mono-articular muscles in which strain might be distributed differently than in longer muscles. Thirdly, the relatively young study population resulted in a majority of less and intermediate affected muscles which has an influence on the average parabolic curvature used as an outcome measure.

To conclude, we have shown a clear non-uniform fat replacement pattern along the proximodistal muscle axis in DMD within individual lower and upper leg muscles. This non-uniformity in fat fraction within an individual muscle has a major influence on quantitative MR measurements and biopsy parameters that are currently considered as outcome measures in clinical trials, and highlights the need for accurate repositioning in longitudinal studies. A slight shift along the proximodistal muscle axis results in a difference in fat fraction which is on average 1–2% ranging up to 12%. These differences are most prevalent in the muscles with intermediate fat fractions. In addition, these findings seem to point to mechanical disruption of the membrane as one of the key factors in the pathophysiology of DMD.

#### Author disclosures

MTH reports a grant from the Netherlands Organization for Health Research and Development (ZonMW) (grant number 113302001) and from the European Union (FP7-HEALTH-2013-INNOVATION-1, grant agreement no. 602485) during conduct of the research. JJGMV and EHN report grants from Duchenne Parent Project, ZonMW and AFM, and trial support from BioMarin, GSK, Lilly and Santhera, outside the submitted work. JJGMV reports grants from European Union and consultancy for Biomarin. EHN reports consultancies for BioMarin and Summit. HEK reports grants from ZonMW, AFM, Duchenne Parent Project, and Gratama Stichting, and consultancy for BioMarin and aTyr Pharma, outside the submitted work. AGW reports grants from NWO and a European Advanced Grant. JB reports a grant from the European Union (FP7-HEALTH-2013-INNOVATION-1, grant agreement no. 602485). CA and EvZ report no disclosures. All reimbursements were received by the LUMC. No personal financial benefits were received.

#### References

- [1] Mendell JR, Shilling C, Leslie ND, et al. A two-tiered approach to newborn screening for Duchenne muscular dystrophy (DMD) using dried blood spots for sequential CK and DNA analysis. *Neuromuscul Disord* 2012;22(9–10):805.
- [2] Straub V, Balabanov P, Bushby K, et al. Stakeholder cooperation to overcome challenges in orphan medicine development: the example of Duchenne muscular dystrophy. *Lancet Neurol* 2016;15(8):882–90.
- [3] Akima H, Lott D, Senesac C, et al. Relationships of thigh muscle contractile and non-contractile tissue with function, strength, and age in boys with Duchenne muscular dystrophy. *Neuromuscul Disord* 2012;22(1):16–25.
- [4] Arpan I, Willcocks RJ, Forbes SC, et al. Examination of effects of corticosteroids on skeletal muscles of boys with DMD using MRI and MRS. *Neurology* 2014;83(11):974–80.
- [5] Willcocks RJ, Forbes SC, Finanger EL, et al. Magnetic resonance imaging and spectroscopy detect changes with age, corticosteroid treatment, and functional progression in DMD. *Neuromuscul Disord* 2013;23(9–10):810.
- [6] Willcocks RJ, Arpan IA, Forbes SC, et al. Longitudinal measurements of MRI-T2 in boys with Duchenne muscular dystrophy: effects of age and disease progression. *Neuromuscul Disord* 2014;24(5):393–401.
- [7] Wokke BH, van den Bergen JC, Versluis MJ, et al. Quantitative MRI and strength measurements in the assessment of muscle quality in Duchenne muscular dystrophy. *Neuromuscul Disord* 2014;24(5):409–16.
- [8] Hollingsworth KG, Garrod P, Eagle M, Bushby K, Straub V. Magnetic resonance imaging in Duchenne muscular dystrophy: longitudinal assessment of natural history over 18 months. *Muscle Nerve* 2013;48(4):586–8.
- [9] Garrod P, Hollingsworth KG, Eagle M, et al. MR imaging in Duchenne muscular dystrophy: quantification of T1-weighted signal, contrast uptake, and the effects of exercise. *J Magn Reson Imaging* 2009;30(5):1130–8.
- [10] Kinali M, Arechavala-Gomez V, Cirak S, et al. Muscle histology vs MRI in Duchenne muscular dystrophy. *Neurology* 2011;76(4):346–53.
- [11] Hogrel JY, Wary C, Moraux A, et al. Longitudinal functional and NMR assessment of upper limbs in Duchenne muscular dystrophy. *Neurology* 2016;86(11):1022–30.
- [12] Wary C, Azzabou N, Giraudeau C, et al. Quantitative NMRS identify augmented disease progression after loss of ambulation in forearms of boys with Duchenne muscular dystrophy. *NMR Biomed* 2015;28(9):1150–62.
- [13] Wary C, Azzabou N, Zehrouni K, et al. One year follow-up of Duchenne muscle dystrophy with nuclear magnetic resonance imaging and spectroscopy indices. *Neuromuscul Disord* 2014;24(9–10):853.
- [14] Bonati U, Hafner P, Schadelin S, et al. Quantitative muscle MRI: a powerful surrogate outcome measure in Duchenne muscular dystrophy. *Neuromuscul Disord* 2015;25(9):679–85.
- [15] Ricotti V, Evans MR, Sinclair CD, et al. Upper limb evaluation in Duchenne muscular dystrophy: fat-water quantification by MRI, muscle force and function define endpoints for clinical trials. *PLoS ONE* 2016;11(9):e0162542.
- [16] Fischmann A, Hafner P, Gloor M, et al. Quantitative MRI and loss of free ambulation in Duchenne muscular dystrophy. *J Neurol* 2013;260(4):969–74.
- [17] Willcocks RJ, Rooney WD, Triplett WT, et al. Multicenter prospective longitudinal study of magnetic resonance biomarkers in a large Duchenne muscular dystrophy cohort. *Ann Neurol* 2016;79(4):535–47.
- [18] Forbes SC, Walter GA, Rooney WD, et al. Skeletal muscles of ambulant children with Duchenne muscular dystrophy: validation of multicenter study of evaluation with MR imaging and MR spectroscopy. *Radiology* 2013;269(1):198–207.
- [19] Janssen BH, Voet NBM, Nabuurs CI, et al. Distinct disease phases in muscles of facioscapulohumeral dystrophy patients identified by MR detected fat infiltration. *PLoS ONE* 2014;9(1):e85416.
- [20] Gaeta M, Mileto A, Mazzeo A, et al. MRI findings, patterns of disease distribution, and muscle fat fraction calculation in five patients with Charcot-Marie-Tooth type 2 F disease. *Skeletal Radiol* 2012;41(5):515–24.
- [21] Rybakova IN, Patel JR, Ervasti JM. The dystrophin complex forms a mechanically strong link between the sarcolemma and costameric actin. *J Cell Biol* 2000;150(5):1209–14.
- [22] Lieber RL, Friden J. Muscle damage is not a function of muscle force but active muscle strain. *J Appl Physiol* 1993;74(2):520–6.
- [23] Morgan DL, Proske U. Popping sarcomere hypothesis explains stretch-induced muscle damage. *Clin Exp Pharmacol Physiol* 2004;31(8):541–5.
- [24] Shin DD, Hodgson JA, Edgerton VR, Sinha S. In vivo intramuscular fascicle-aponeuroses dynamics of the human medial gastrocnemius during plantarflexion and dorsiflexion of the foot. *J Appl Physiol* 2009;107(4):1276–84.
- [25] van den Bergen JC, Ginjaar HB, van Essen AJ, Pangalila R, de Groot IJ, Wijkstra PJ. Forty-five years of Duchenne muscular dystrophy in the Netherlands. *J Neuromuscul Dis* 2014;1:99–109.

- [26] Yu HZ, Shimakawa A, McKenzie CA, Brodsky E, Brittain JH, Reeder SB. Multiecho water-fat separation and simultaneous R-2\* estimation with multifrequency fat spectrum modeling. *Magn Reson Med* 2008;60(5): 1122–34.
- [27] Loughran T, Higgins DM, McCallum M, Coombs A, Straub V, Hollingsworth KG. Improving highly accelerated fat fraction measurements for clinical trials in muscular dystrophy: origin and quantitative effect of R2\*changes. *Radiology* 2015;275(2):570–8.
- [28] Fischmann A, Gloor M, Fasler S, et al. Muscular involvement assessed by MRI correlates to motor function measurement values in oculopharyngeal muscular dystrophy. *J Neurol* 2011;258(7):1333–40.
- [29] Sinclair CDJ, Morrow JM, Miranda MA, et al. Skeletal muscle MRI magnetisation transfer ratio reflects clinical severity in peripheral neuropathies. *J Neurol Neurosurg Psychiatry* 2012;83(1):29–32.
- [30] Hafner P, Bonati U, Erne B, et al. Improved muscle function in Duchenne muscular dystrophy through L-arginine and metformin: an investigator-initiated, open-label, single-center, proof-of-concept-study. *PLoS ONE* 2016;11(1):e0147634.
- [31] Samitt CE, Bonilla E. Immunocytochemical study of dystrophin at the myotendinous junction. *Muscle Nerve* 1990;13(6):493–500.
- [32] Atsuta F, Sato K, Maruyama K, Shimada Y. Distribution of connectin (titin), nebulin and alpha-actinin at myotendinous junctions of chicken pectoralis-muscles – an immunofluorescence and immunoelectron microscopic study. *J Muscle Res Cell Motil* 1993;14(5):511–17.
- [33] Moens P, Baatsen PHWW, Marechal G. Increased susceptibility of EDL muscles from Mdx mice to damage-induced by contractions with stretch. *J Muscle Res Cell Motil* 1993;14(4):446–51.
- [34] Hu X, Blemker SS. Musculoskeletal simulation can help explain selective muscle degeneration in Duchenne muscular dystrophy. *Muscle Nerve* 2015;52(2):174–82.